Contribution of primary and scattered photons in EPID images in RT

Author: Martí Foix Pérez
Facultat de Física, Universitat de Barcelona, Diagonal 645, 08028 Barcelona, Catalonia, Spain

Advisors: Dr. José M. Fernández-Varea
Departament de Física Quàntica i Astrofísica

Artur Latorre Musoll
Hospital de la Santa Creu i Sant Pau. Servei de Radiofísica i Radioprotecció

Abstract: In this final degree project we have studied the contribution of the different components of radiation in EPID images. We have used the PENELOPE/penEasy code to simulate various situations in which the patient is displaced. Knowing how the different components behave, we can apply a mathematical model that allows us to estimate the displacement of the patient from the EPID image.

I. INTRODUCTION

Radiotherapy is an oncological treatment modality that uses high absorbed doses of ionizing radiation to eliminate cancer cells and shrink tumours. Bremsstrahlung x-rays are the most common type of ionizing radiation employed, but electrons and even protons and carbon ions can also be used. When treating a patient, it is as equally important to deliver the prescribed dose as to deliver the radiation to the correct anatomical site, so the surrounding healthy tissues are not harmed. Before the treatment, techniques such as cone-beam computed tomography are commonly used to verify the patient's correct positioning, but we cannot control if the patient moves during the treatment. Traditionally, Surface-Guided Radiation Therapy (SGRT) and Image-Guided Radiation Therapy (IGRT) techniques, as well as industrial x-ray film have been used to ensure the patient positioning during the treatment. However, film needs to be processed so the information is only available once the treatment session is finished, and the equipment required for SGRT and IGRT is expensive. In recent years, electronic portal imaging devices (EPIDs) have been developed and have been the preferred tools for the instantaneous verification of the patient positioning [1, 2].

In order to verify that the patient is receiving the correct absorbed dose during the treatment, it is advantageous to determine the dose from transmission images, which are acquired using the treatment x-ray beam after it passes through the patient and reaches the detector [2]. These images are known as portal images. The aim of this project was to study, with Monte Carlo simulations, how the different components of radiation contribute to EPID imaging. The PENELOPE/penEasy code allows us to filter the photons arriving at the detector according to the interactions they have undergone. We have studied each component separately for five arbitrary patient displacements and four gantry orientations for clinically representative radiation fields, adopting an anthropomorphic phantom as patient.

II. MATERIALS AND METHODS

A. Photon interactions

Photons interact with the patient resulting in different components of radiation. On the one hand we have Rayleigh scattering, the process by which a photon is elastically scattered by bound atomic electrons. Radiation used in radiotherapy are usually megavoltage (MV) beams, so we have to evaluate the Rayleigh scattering cross section, σ_{R}, in the high-energy limit [3]

$$\sigma_{\mathrm{R}} \propto Z^2\, E^{-2}. \tag{1}$$

On the other hand, there is Compton scattering. In the Compton effect, a photon with energy E is absorbed by an atomic electron and another photon with energy $E' < E$ is emitted at an angle θ with respect to the direction of the primary photon. The Compton cross section per atom, σ_{C}, for MV photon beams can be approximated in terms of the Klein–Nishina cross section σ_{KN} as [3]

$$\sigma_{\mathrm{C}} \approx Z\, \sigma_{\mathrm{KN}} \sim Z\, E^{-1}. \tag{2}$$

Not all photons reach the detector, some of them are absorbed by photoelectric effect with a cross section $\sigma_{\mathrm{pe}} \propto Z^5\, E^{-7/2}$, and some disappear producing an electron-positron pair, with a cross section given by the Bethe–Heitler formula [3]

$$\frac{\mathrm{d}\sigma_{\mathrm{BH}}}{\mathrm{d}E_-} = Z(Z+1)\, f(Z, E; E_-), \tag{3}$$

where E_- is the kinetic energy of the resulting electron.

As we can see, the Rayleigh cross section decreases faster than Compton's with energy, so we can anticipate that the Compton effect will be the predominant interaction but, since it also decreases with energy and we are using MV radiation, the contribution will be negligible with respect to the unscattered photons.

B. Monte Carlo simulations

As mentioned above, we used the PENELOPE code for Monte Carlo simulations. PENELOPE stands for PENetration and Energy LOss of Positrons and Electrons. There are three types of input file required to run a simulation: geometry files, material files and configuration files.

Geometry files contain information of the surfaces and bodies radiation is going to cross, in our case the EPID and the anthropomorphic phantom. There are three possible models of geometry: quadric geometries, voxelized geometries and a combination of both.

Quadric geometries are based on quadric surfaces, defined by the expression

$$I_1\,x^2 + I_2\,y^2 + I_3\,z^2 + I_4\,z + I_5 = 0 \tag{4}$$

with $I_i = 0, \pm 1$ [3]. After a surface is defined it can be scaled, rotated and/or translated. Once we have defined the surfaces, we can create bodies delimited by these surfaces and assign them a specific material. Bodies can be grouped in modules. Quadric geometry files are named with extension *.geo.

Voxelized geometries are a collection of small cuboid volume elements with a homogeneous material composition and mass density. All voxels have the same dimensions and are adjacent, except for the voxels located in the periphery. The voxels have each side parallel to one of the Cartesian axis of the lab reference frame. Voxelized geometry files are named with extension *.vox and in most cases they will be created by a program processing a CT scan [4].

Our (simplified) EPID is a $32.5 \times 32.5 \times 1$ cm^3 parallelepiped defined by six quadric surfaces. The anthropomorphic phantom is defined by a voxelized geometry.

As we said, bodies and modules have materials assigned. The properties of each material (atomic number, mass density, cross sections, ...) are stored in the material files, and each material has its own file, with extension *.mat. To generate a material file we use the auxiliary executable *material.exe*, which allows to select one of the 280 materials available in PENELOPE's database or to enter the composition data from the keyboard.

In our case, we used six material files from the database: ultra low-density hydrogen (modified from the database) used as pseudo-vacuum and ideal detector, air, lung, adipose tissue, muscle skeletal and cartilage and bone compact.

The configuration file, with extension *.in, is where we define settings such as the desired number of histories or allotted time, the properties of the radiation source, the geometry and material files, the transport parameters, ... We also select the *tallies* we want to activate to produce the output information.

As for the radiation transport parameters, we have defined the detector as a perfect absorber, hence the absorption energies (below which the program ceases to simulate the particles) were set to $E_{\text{abs}} = 1$ GeV for all photons, electrons and positrons. For the other materials, $E_{\text{abs}} = 10$ keV for photons and $E_{\text{abs}} = 500$ keV for electrons and positrons. We have also set a cutoff value for hard collisions of $W_{\text{cc}} = 1$ keV and a cutoff for bremsstrahlung emission of $W_{\text{cr}} = 10$ keV.

As for the *tallies*, we have only employed the *Tally Pixelated Imaging Detector* which creates a pixelated image of the radiation field that reaches the detector. This tally allows us to filter radiation in five components:

- **Unscattered**: Photons emitted from the source that reach the detector without having undergone any interaction.
- **Rayleigh**: Photons that have undergone exactly one Rayleigh interaction before reaching the detector.
- **Compton**: Photons that have undergone exactly one Compton interaction before reaching the detector.
- **Secondaries**: Photons that were not emitted from the source, but were created as a result of an interaction.
- **Multiscattered**: Photons that have experienced more than one interaction, or secondaries that have experienced at least one interaction.

The image is reported as a matrix of pixels, each of which can be understood as an elemental detector.

There are three detection modes: energy integrating, photon counting and pulse-height spectrum (energy discriminating). We chose the energy integrating mode, in which the reported image is the energy deposited in each pixel per unit area and history. In photon counting and energy discriminating modes, we would define an energy interval $(E_{\text{min}}, E_{\text{max}})$. In photon counting mode the signal is the number of counts per history in which the energy falls in this interval. In energy discrimination mode the energy deposited is classified into bins that cover the interval $(E_{\text{min}}, E_{\text{max}})$. The signal in each pixel is the number of counts per history in each energy bin, divided by the bin width.

C. Phase-space files

PRIMO [5] is a software that simulates linacs. It combines a graphical user interface with the PENELOPE code for radiation transport. It includes a version of the Dose Planning Method code (DPM v1.1) [6] which simulates absorbed dose distributions in external-beam radiotherapy treatments [7].

The simulation in PRIMO is divided in segments, as shown in figure 1. The first segment, s1, simulates the primary electron beam producing bremsstrahlung radiation. The second segment, s2, is where the field configuration is set. This segment simulation setup includes the

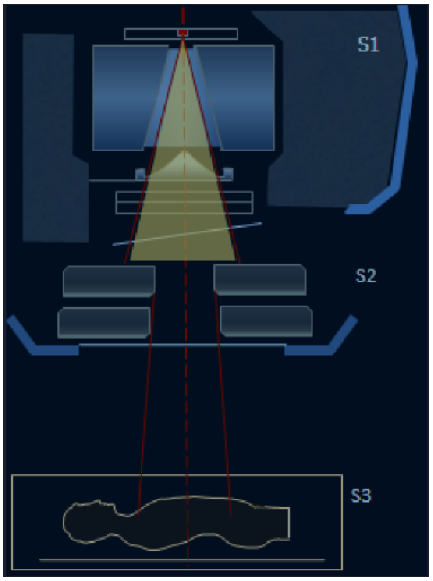

FIG. 1: Schematic representation of the linac in PRIMO workspace where the first segment has been selected.

position of the jaws and the multileaf collimator, as well as the gantry and couch rotation and the isocenter position in the patient. The third segment, s3, starts when the radiation leaves the linac.

When simulating with PRIMO, it is possible to record the state of the particles crossing a plane at the end of segments s1 and s2. This information is written on a file called phase-space file (PSF). We have been provided four PSFs corresponding to four gantry orientations by Hospital de la Santa Creu i Sant Pau. These PSFs were our radiation sources for the simulations.

In our simulations, s1 and s2 are always the same for each gantry rotation, hence the four PSFs were recorded at the end of s2, containing information such as energy, position or direction of flight of the photons leaving the accelerator. The PSFs were provided to us by Artur Latorre (Hospital de la Santa Creu i Sant Pau) because of the large amount of CPU needed, unavailable in a regular personal computer such as the one used in this project.

D. Beer–Lambert law

The Beer–Lambert law relates the attenuation of light to the properties of the material through it is travelling. Being $D(x, y)$ the matrix for a direct portal image; *i.e.*, an image of the radiation field without a patient or a phantom, $T(x, y)$ the transit portal image (with the patient or phantom), μ the average mass attenuation coefficient and $t(x, y)$ the mass thickness, the Beer–Lambert law is written as

$$T(x, y) = D(x, y)\, \mathrm{e}^{-\mu t(x,y)}. \tag{5}$$

If we now introduce a displacement, the new mass thickness, in a first-order approximation, is given by

$$t(x, y) \simeq t_0(x, y) - \vec{\mathbf{s}} \cdot \vec{\nabla} t_0(x, y), \tag{6}$$

where $\vec{\mathbf{s}}$ is the displacement vector projected to the EPID plane. Using equations (5) and (6), we can write the transit image after a displacement as

$$T \simeq D\, \mathrm{e}^{-\mu t_0}(1 + \mu \vec{\mathbf{s}} \cdot \vec{\nabla} t_0) = T_0(1 + \mu \vec{\mathbf{s}} \cdot \vec{\nabla} t_0), \tag{7}$$

where we applied a first order-approximation for a small $\vec{\mathbf{s}}$ and T_0 is the non-displaced transit image. The only unknown variable in this equation is the displacement vector $\vec{\mathbf{s}}$. We can rewrite equation (7) as

$$\vec{\mathbf{s}} \cdot \vec{\nabla} t_0 = (\mu T_0)^{-1} (T - T_0). \tag{8}$$

The Beer–Lambert law is valid only for unscattered radiation, hence we have to verify that the scattered components of radiation are negligible.

We have chosen five arbitrary displacement vectors $\vec{\mathbf{S}}$ of module around 1 cm: $(1, 0, 0)$, $(0, 1, 0)$, $(0.5, -0.5, 0.5)$, $(0.8, -0.2, -0.1)$, $(-0.3, 0.7, 0)$; and we have performed six simulations for each displacement and for a perfectly positioned patient (one with no filter applied and one for each filter). Additionally, we have repeated the process for four different PSFs corresponding to four gantry rotations (60^{o}, 85^{o}, 120^{o} and 180^{o}) to be sure the results are similar. This entailed a total of 144 simulations.

Once we completed all the simulations, we integrated all pixels of each image and calculated the relative average intensity value per component. Furthermore, using the proportionality of $\vec{\mathbf{S}}$ with the subtraction $(T - T_0)$, equation (8), we could study this subtraction separately for unscattered and scattered components.

III. RESULTS AND DISCUSSION

First of all, we need to point out that, due to the lack of time, the simulations were performed with a splitting factor of 1. The splitting factor is a factor F that replicates every particle from the PSF F times. Each replica has a statistical weight of $1/F$. By increasing the splitting factor, variance is reduced.

After verifying that the sum of the five images corresponding to each component of radiation was equivalent to the image with no filter we started simulating the displacements.

Figures 2 and 3 are two examples of recorded images, the first one corresponding to a perfectly positioned patient and the second one pertaining to a displacement. We can observe slight differences between both, showing that the dose distribution is not the same.

A. Contribution of the components

To analyze the contribution of the components of radiation, we have integrated all the pixels of the non-

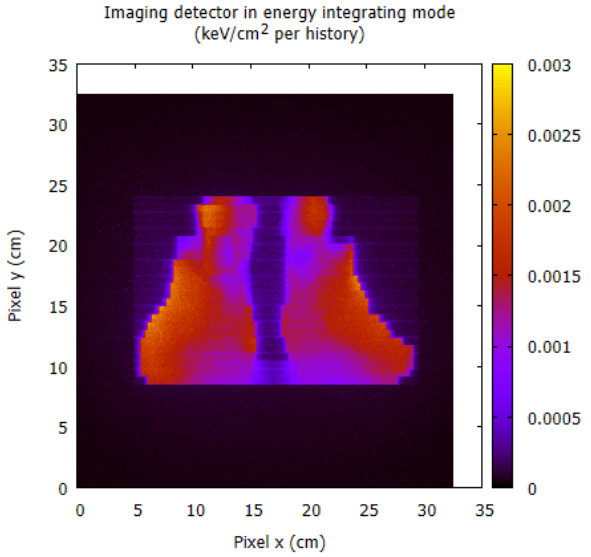

FIG. 2: Image for the 180º PSF with no filter applied and $\vec{\mathbf{S}} = \vec{0}$.

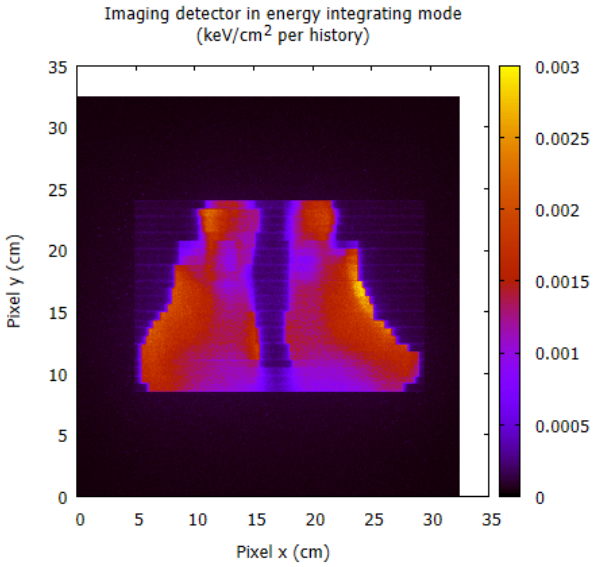

FIG. 3: Image for the 180º PSF with no filter applied and $\vec{\mathbf{S}} = (0.8, -0.2, -0.1)$.

displaced images and we have calculated the average value. The results are summarized in table I.

The unscattered component is dominant, but Compton scattering has a significant contribution. However, figures 2 and 3 clearly show a central rectangular area that corresponds to the region irradiated with a high dose, where we should focus. In a second analysis, we have calculated the average value only in this central area.

In this second analysis the Compton contribution has decreased with respect to the first analysis, and the unscattered contribution is even more dominant, as shown in table II. This justifies using models that describe unscattered behavior (*e.g.*, the Beer–Lambert law), even though the image has other components which behave otherwise. We have repeated the same analysis for all the displacement vectors, and the results are similar in every case.

TABLE I: Contributions of the different components of radiation in the images with no displacement.

PSF	Unscat.	Rayleigh	Compton	Second.	Multisc.
60º	84.94 %	0.03 %	12.44 %	0.08 %	2.51 %
85º	85.08 %	0.03 %	12.32 %	0.08 %	2.49 %
120º	86.82 %	0.03 %	11.00 %	0.07 %	2.08 %
180º	88.10 %	0.03 %	9.95 %	0.06 %	1.86 %

TABLE II: Contributions of the different components of radiation in the high dose irradiated area of the images with no displacement.

PSF	Unscat.	Rayleigh	Compton	Second.	Multisc.
60º	92.61 %	0.03 %	6.16 %	0.03 %	1.17 %
85º	93.91 %	0.03 %	5.15 %	0.03 %	0.88 %
120º	93.87 %	0.03 %	5.22 %	0.03 %	0.85 %
180º	93.10 %	0.03 %	5.84 %	0.03 %	1.00 %

B. Subtraction $T - T_0$

It is interesting to study the subtraction in equation (8) separately for unscattered and scattered components. To simplify, we have added all the scattered components into a single one.

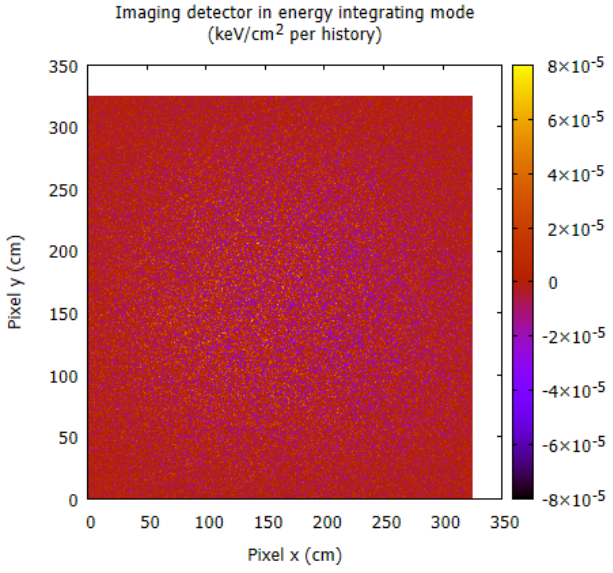

FIG. 4: Subtraction of the scattered components of the simulation with $\vec{\mathbf{S}} = \vec{0}$ with respect to the simulation with $\vec{\mathbf{S}} = (0.8, -0.2, -0.1)$ for the 180º PSF.

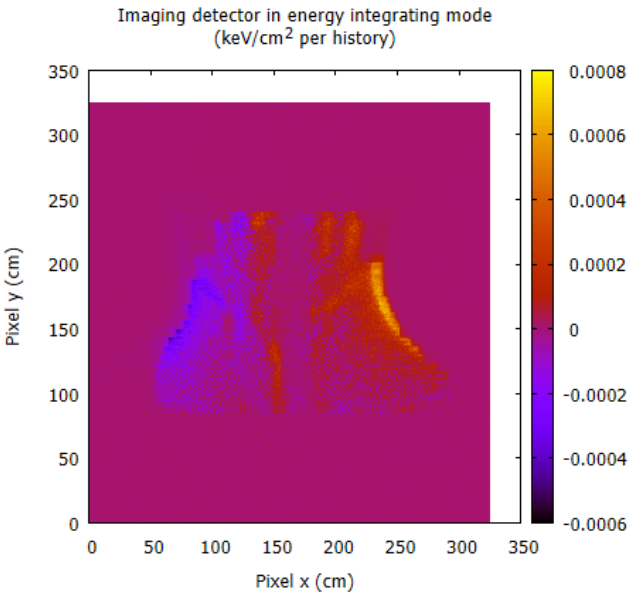

FIG. 5: Subtraction of the unscattered components of the simulation with $\vec{\mathbf{S}} = \vec{0}$ with respect to the simulation with $\vec{\mathbf{S}} = (0.8, -0.2, -0.1)$ for the 180º PSF.

Figure 4 is the subtraction of the scattered components of figures 2 and 3. By doing this subtraction to find the displacement, the small contribution of the scattered components is statistically eliminated.

Figure 5 is the unscattered component of the same subtraction. This subtraction maintains the information of the difference in dose distribution between figures 2 and 3. This reinforces the validity of the Beer–Lambert law in this case, considering that the subtraction cancels the scattered contributions.

We obtained the same results for all the displacements and every PSF.

IV. CONCLUSIONS

Notwithstanding that if we had used a larger splitting factor the simulations would have been more realistic and the variance would have been reduced, we obtained the expected results. The unscattered component of radiation is predominant, especially in the high dose irradiated area. Moreover, when we use the Beer–Lambert law to determine the displacement, we don't use single images, but differences with respect to a reference image, in this case the image for a perfectly positioned patient. In this differences, the only component of radiation that provides us information of the changes in dose distribution is the unscattered. This means that besides the fact that the scattered components have a small contribution to the images, it is statistically eliminated. Hence, we can apply the Beer–Lambert law regardless of only being valid for unscattered radiation.

With these results, we can conclude that this model can be applied in the algorithm developed by Artur Latorre at the Hospital de la Santa Creu i Sant Pau, the goal of which is to determine the displacement of the patient from the EPID image.

Acknowledgments

I am very grateful to my advisors José M. Fernández-Varea and Artur Latorre for all their assistance and guidance. I would like to thank my partner, Judith Cabello, for all her support; and my friends and colleagues, particularly Macià Mut, Miquel Tomé and Jordi Mangues. Last but not least, I want to thank my parents, Toni and Carolina, and my brother Ernest.

[1] *Handbook of Radiotherapy Physics*. Edited by P. Mayles, A. Nahum and J. C. Rosenwald. (Taylor & Francis Group, 2007) chapter 14.

[2] W. van Elmpt, L. McDermott, S Nijsten, M. Wendling, P. Lambin and B. Mijnheer, A literature review of electronic portal imaging for radiotherapy dosimetry, *Radiother. Oncol.* **88** (2008) 289–309.

[3] F. Salvat, *PENELOPE, a Code System for Monte Carlo Simulation of Electron and Photon Transport* (OECD/NEA, 2019) chapters 2 and 6.

[4] J. Sempau, A. Badal and L. Brualla, A PENELOPE-based system for the automated Monte Carlo simulation of clinacs and voxelized geometries–application to far-from-axis fields, *Med. Phys.* **38** (2011) 5887–5895.

[5] M. Rodriguez, J. Sempau and L. Brualla, PRIMO: A graphical environment for the Monte Carlo simulation of Varian and Elekta linacs, *Strahlenther. Onkol.* **189** (2013) 881–886.

[6] J. Sempau, S. J. Wilderman and A. F. Bielajew, DPM, a fast, accurate Monte Carlo code optimized for photon and electron radiotherapy treatment planning dose calculations, *Phys. Med. Biol.* **45** (2000) 2263–2291.

[7] M. Rodriguez, J. Sempau, C. Bäumer, B. Timmermann and L. Brualla, DPM as a radiation transport engine for PRIMO, *Radiat. Oncol.* **13** (2018) 256.